Chemistry SELECT

Supporting Information

Role of Anomalous Water Constraints in the Efficacy of Pharmaceuticals Probed by ^{1}H Solid-State NMR

Joshua T. Damron[+], Kortney M. Kersten[+], Manoj Kumar Pandey, Yusuke Nishiyama, Adam Matzger,* and Ayyalusamy Ramamoorthy*

Table of Contents

SI 1. Experimental Procedures

Experimental Section

Materials

Mercaptopurine monohydrate, deuterated methanol (MeOD), and D_2O were obtained from Acros. Methanol was obtained from Fisher Scientific. All reagents were used without further purification. The purity of the material, from which the hydrates were made, as received from the distributor is 99.5%.

Crystallization

Crystallization of the hydrates were produced in the manner reported by Kersten et. al.[1] Crystals of the monohydrate form were grown from methanol solutions (4 mg/mL) heated to 80 °C to dissolve all solids. Solutions were passed through a syringe filter (9 mL) into a 20 mL vial containing 5 mL H_2O. Vials were sealed and yellow block-shaped crystals grew after two days at room temperature. Crystals of the hemihydrate form were grown from methanol solutions (4 mg/mL) heated to 80 °C to dissolve all solids. Solutions were passed through a syringe filter (4.5 mL) into a 20 mL vial containing 0.5 mL H_2O. Vials were sealed and yellow needle crystals grew after two days at room temperature.

Samples of both the monohydrate and hemihydrate forms were also created using MeOD and D_2O to crystallize samples with deuterated nitrogens and water molecules (See Section S4, Figure S8)

Infrared Spectroscopy

Fourier transform infrared spectroscopy analyses were performed on the hemihydrate and monohydrate forms of mercaptopurine using an attenuated total reflectance accessory (ATR; ThermoNicolet Avatar model 360-FTIR). The scan range was 680 to 4000 cm^{-1}, employing 512 scans with a resolution of 4 cm^{-1}. Samples were analyzed on the ATR stage and the empty stage was used as the blank.

NMR Spectroscopy

All mercaptopurine CSA/CS data were acquired on a JEOL ECZ600R at 600 MHz ^{1}H Larmor frequency using a JEOL RESONANCE Inc. 0.75 mm double-resonance MAS probe under 90 kHz +/- 20 Hz MAS at room temperature (25 °C). Six scans were used with a recycle delay of 120 s and 32 t_1 points in all experiments. The decoupled spectra were obtained with ^{14}N-^{1}H decoupling (99W/~117 kHz) using an on-resonance ^{14}N irradiation during the ^{1}H CSA recoupling t_1 period to avoid the reintroduction of ^{14}N-^{1}H dipolar interactions.

2D CS/CSA pulse sequence

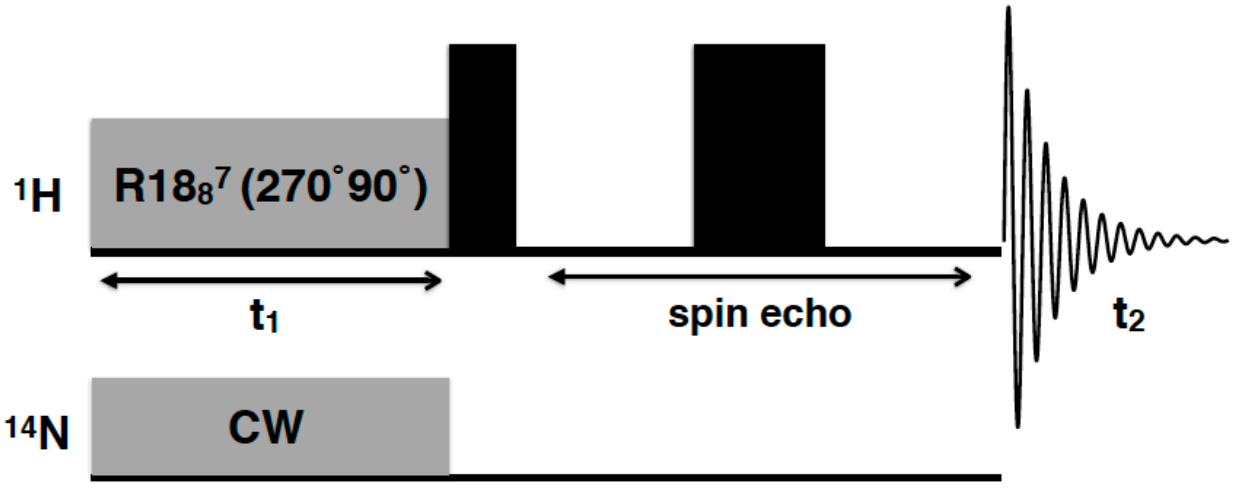

Figure S1. Schematic of the radio-frequency pulse sequence used for all CS/CSA correlations experiments. The solid black rectangles in the ^{1}H RF channel are 90° and 180° pulses.

The pulse sequence[2,3] used for CSA/CS correlation depicted in Figure S1 is a gamma-encoded symmetry based pulse sequence for selective recoupling of the ^{1}H CSA anisotropy. The notation $R18_8^7(270°90°)$ comes from the symmetry principles for pulse sequence design introduced by Levitt and co-workers.[4,5] The general notation RN_n^v refers to N, the number of phase-alternated composite pulses, n the number of rotor periods, and v determines the phase of the pulses by $\pi v/N$. In this case, (270°90°) is a composite 180° pulses whose phase alternates between (70°, 250°) and (-70°, -250°). The proper choice of N, n and v determine which interactions are retained according to the symmetry of the first-order Hamiltonian. In this case, the symmetry renders the CSA and heteronuclear dipolar couplings. To limit the evolution in t_1 strictly to CSA, heteronuclear

decoupling is applied on the ^{14}N channel. This is necessary for abundant hetero-nuclei, such as ^{14}N. Given the low natural-abundance of ^{13}C and ^{15}N, it is not necessary to apply decoupling on these RF channels, as only very small fractions of ^{1}H spins are affected. The proton magnetization is then refocused by a spin-echo to suppress background signals and then detected in the t_2 period where the isotropic chemical shift is encoded in the magnetization. The experimentally measured spectrum gives a bimodal line-shape in the t_1 dimension whose splitting is roughly proportional to the magnitude of the CSA, while the shape of the line is related to the asymmetry parameter, or shape of the CSA tensor. The experimentally measured line-shapes are numerically simulated using SIMPSON software to extract the CSA and asymmetry parameters. The reported SS NMR parameters are the CSA, defined as $\zeta = \delta_{zz} - \delta_{iso}$, and the asymmetry parameter $\eta = (\delta_{xx} - \delta_{yy})/\zeta$, where δ_{iso} is the trace of the CSA tensor (or the isotropic chemical shift), and δ_{ii} are its principal components ordered as $|\delta_{zz} - \delta_{iso}| \geq |\delta_{xx} - \delta_{iso}| \geq |\delta_{yy} - \delta_{iso}|$.

Charge Density Map Calculations

Computation of the charge density maps of the two tautomeric forms of mercaptopurine were performed in Spartan '14 V 1.1.2. The energy of the initial structure was minimized using molecular mechanics (MMFF). The equilibrium geometry was calculated using density functional theory B3LYP with the basis set 6-31G* in the gas phase. The electrostatic potential map surface was calculated and then displayed.

Geometry optimization was first performed on all structures where all atoms except hydrogen were held at a constant position. The unit cell parameters were also held constant, and the calculations were performed using an ultra-fine quality with the COMPASS II force field assigned, which is parameterized for the functional groups present. This initial optimization gave the total energy for the initial crystal structures containing the water molecules. For both the hemi and monohydrate systems, the water molecules were deleted and energy calculations were performed again using the COMPASS II force field assigned to give a total energy for the system after theoretical water loss. Density functional theory calculations were also performed before and after deletion of the water molecules for each structure using two different modules. Preoptimization of the structures was performed using the only H free molecular mechanics method above. For the CASTEP module, ultrafine energy calculations were then performed using the GGA-PW91 theory. This gave the energy for the system containing water molecules. The water molecules were then deleted and energy calculations were performed again using the GGA-PW91 theory to give the energy for the system after theoretical water loss. For the Dmol3 module, fine geometry optimization calculations with the GGA-PW91 theory were performed on the preoptimized structures using the only H free molecular mechanics method above. The water molecules were then deleted and fine energy calculations were performed again using the GGA-PW91 theory to determine the energy for the system after theoretical water loss. Figure S9 and Tables S4 and S5 show the above-mentioned free energy values and the method and results for the calculation of theoretical desolvation energies for each form.

Calculated IR Spectroscopy Stretches

The theoretical IR stretches for both the monohydrate and hemihydrate forms of mercaptopurine were calculated using DFT calculations in Materials Studio 7.0. The same geometry optimizations were performed following the desolvation energy calculations above; first by using Molecular Mechanics (Forcite with COMPASS II) and then DFT (Dmol3) to get an optimized structure of each form. The frequency values of each form were then calculated using DFT methods by way of medium frequency analysis as a property in the Dmol3 calculation using the GGA-PW91 theory. Vibrational analysis was performed, the modes were calculated, and the frequencies were animated to determine the appearance of OH stretches of each hydrate form.

SI 2. Pharmaceutical Hydrate Statistics

Table S1. Database of pharmaceutical compounds created from listings of the top selling pharmaceuticals by prescriptions from 2005-2015.[6–11]

	Pharmaceutical (Brand Name)	**Solid form**
1	Abilify	Anhydrate
2	Aciphex	Salt
3	Actonel	Salt
4	Actos	Salt
5	Adderall XR	Salt
6	Advair	Salt and Anhydrate
7	Afinitor	Anhydrate
8	Allegra	Salt
9	Allegra-D	Salts
10	Altace	Anhydrate
11	Amaryl	Anhydrate
12	Ambien	Salt
13	Anoro Ellipta	Salts
14	Aricept	Salt
15	Armour Thyroid	Anhydrates
16	Atripla	Salt and Anhydrates
17	Avalide	Anhydrates
18	Avandia	Salt
19	Avapro	Anhydrate
20	Avelox	Salt
21	Aviane/ Seasonique	Anhydrates
22	Belviq	Salt Hydrate (Hemi)
23	Benicar	Anhydrate
24	Benicar HCT	Anhydrates
25	Boniva	Salt Hydrate (Mono)

26	Breo Ellipta	Salt and Anhydrate
27	Brisdelle	Salt
28	Budeprion SR/ Wellbutrin XL	Salt
29	Bystolic	Salt
30	Caduet	Salt and Salt Hydrate (Tri)
31	Celebrex	Anhydrate
32	Chantix	Salt
33	Cialis	Anhydrate
34	Clarinex	Anhydrate
35	Combivent	Salt and Salt Hydrate (Mono)
36	Complera	Anhydrate and Salts
37	Concerta/ Quillivant XR	Salt
38	Coreg	Anhydrate
39	Coumadin	Salt
40	Cozaar	Salt
41	Crestor	Salt
42	Cymbalta	Salt
43	Depakote ER	Salt
44	Detrol LA	Salt
45	Dexilant	Anhydrate
46	Digitek/ Lanoxin	Anhydrate
47	Diovan	Anhydrate
48	Diovan HCT	Anhydrates
49	Duavee	Salt and Anhydrate
50	Dulera	Anhydrate and Salt Hydrate (Di)
51	Effexor XR	Salt
52	Eliquis	Anhydrate
53	Endocet	Salt and Anhydrate
54	Evista	Salt
55	Farxiga	Hydrate (Mono) Solvate (1,2Propanediol)
56	Flomax	Salt
57	Flovent/ Flonase	Anhydrate
58	Focalin	Salt
59	Fosamax	Salt Hydrate (Tri)
60	Geodon Oral	Salt Hydrate (Mono)
61	Gilenya	Salt
62	Gleevec	Salt
63	Glipizide XL	Anhydrate
64	Hyzaar	Salt and Anhydrate
65	Imitrex	Salt
66	Intuniv	Salt

67	Invega Sustenna	Anhydrate
68	Invokana	Hydrate (Hemi)
69	Isentress	Salt
70	Janumet	Salt and Salt Hydrate (Mono)
71	Januvia	Salt Hydrate (Mono)
72	Kariva	Anhydrates
73	Klor-Con	Salt
74	Lamictal	Anhydrate
75	Latuda	Salt
76	Levaquin	Hydrate (Hemi)
77	Levitra	Salt Hydrate (Tri)
78	Lexapro	Salt
79	Lipitor	Salt Hydrate (Tri)
80	Livalo	Salt
81	Loestrin 24 Fe	Anhydrate and Salt
82	Lotrel	Salts
83	Lunesta	Anhydrate
84	Lyrica	Anhydrate
85	Micardis	Anhydrate
86	Mirapex	Salt Hydrate (Mono)
87	Mobic	Anhydrate
88	Monodox	Hydrate (Mono)
89	Myrbetriq	Anhydrate
90	Namenda	Salt
91	Nasacort AQ	Anhydrate
92	Nasonex	Hydrate (Mono)
93	Nexium	Salt Hydrate (Tri)
94	Niaspan	Anhydrate
95	Norvasc	Salt
96	Omnaris	Anhydrate
97	Omnicef	Anhydrate
98	Onglyza	Salt Hydrate (Mono)
99	Ortho Evra/Trinessa/Tri-Sprintec/Yasmin 28	Anhydrates
100	Osphena	Anhydrate
101	Oxycontin	Salt
102	Paxil CR	Salt Hydrate (Hemi)
103	Plavix	Salt
104	Pradaxa	Salt
105	Pravachol	Salt
106	Premarin	Anhydrate
107	Prempro	Anhydrates

108	Prevacid	Anhydrate
109	Prezista	Solvate (Ethanol)
110	Prilosec	Anhydrate
111	Pristiq	Salt Hydrate (Mono)
112	Proair/ Proventil/ Ventolin HFA	Salt
113	Protonix	Salt Hydrate (Sesqui)
114	Provigil	Anhydrate
115	Relpax	Salt
116	Requip	Salt
117	Reyataz	Salt
118	Rhinocort Aqua	Anhydrate
119	Risperdal	Anhydrate
120	Sensipar	Salt
121	Seroquel	Salt
122	Singulair	Salt
123	Skelaxin	Anhydrate
124	Solodyn	Salt
125	Sovaldi	Anhydrate
126	Spiriva	Salt Hydrate (Mono)
127	Strattera	Salt
128	Stribild	Anhydrates and Salt
129	Suboxone	Salt and Salt Hydrate (Di)
130	Symbicort	Salt Hydrate (Di) and Anhydrate
131	Synthroid/ Levoxyl/ Levothyroid	Salt Hydrate (Channel)
132	Tamiflu	Salt
133	Tecfidera	Anhydrate
134	Topamax	Anhydrate
135	Toprol XL	Salt
136	Toviaz	Salt
137	Tricor	Anhydrate
138	Trilipix	Salt
139	Truvada	Salt and Anhydrate
140	Tussionex	Salts
141	Uloric	Anhydrate
142	Valtrex	Salt
143	Vesicare	Salt
144	Viagra	Salt
145	Vicodin	Anhydrate and Salt Hydrate (2.5)
146	Vimovo	Anhydrate and Salt Hydrate (Tri)
147	Vytorin	Anhydrates
148	Vyvanse	Salt

149	Xarelto	Anhydrate
150	Xeljanz	Salt
151	Xeloda	Anhydrate
152	Xopenex	Salt
153	Yaz-28	Anhydrates
154	Zetia	Anhydrate
155	Zithromax	Hydrate (Di)
156	Zocor	Anhydrate
157	Zoloft	Salt
158	Zyprexa	Anhydrate
159	Zyrtec	Salt
160	Zyrtec-D	Salts
161	Zytiga	Anhydrate

Table S2. Statistical data for each solid form type from the database in table S1.

	Hydrates	Salt Hydrates	Salts	Anhydrates	Total
Total	6	23	75	56	160
Percent	3.75	14.38	46.88	35.00	100.01

SI 3. Supporting NMR Data

Additional NMR experiments were performed for resonance assignment. First, the hydrates were prepared using MeOD and D_2O, which replace the water molecules as well as exchange the NH protons revealing only the aromatic resonances in the ^1H spectrum. Figure S7 (c and d) shows the deuterated samples, confirming the aromatic position at slightly above 8 ppm for both hydrate forms. For comparison, the fully protonated 1D spectra are shown in the top part of Figure S7 (a and b).

In addition, the CSA measurements were run without ^{14}N decoupling, allowing the through space ^{14}N-^1H heteronuclear dipolar interaction to also contribute the line-shape as well as the CSA. As such, a comparison of the two allows for easy identification of the NH resonances. Figure S8 shows this comparison where the most downfield resonances in both cases are severely broadened by the lack of decoupling, confirming the NH resonance assignments. The CSA numbers including with and without decoupling are summarized in Table S3. The NH resonances are so distorted their lines could not be fit.

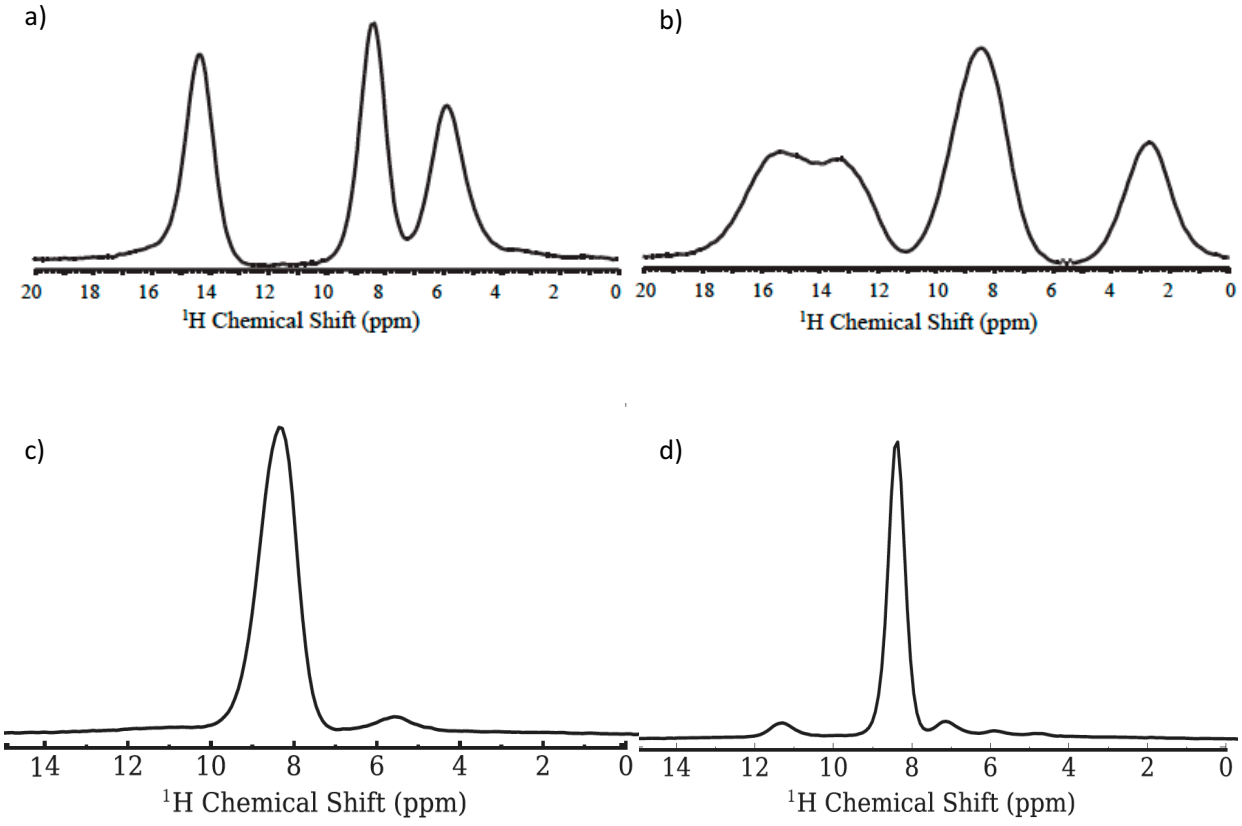

Figure S2. ^1H spin-echo of mercaptopurine: (a) monohydrate with H_2O, (b) hemihydrate with H_2O, (c) monohydrate with MeOD/D_2O and (d) hemihydrate with MeOD/D_2O. The H/D exchange was used for confirmation of exchangeable peaks. By this method, all NH and OH hydrogens are replaced with deuterium.

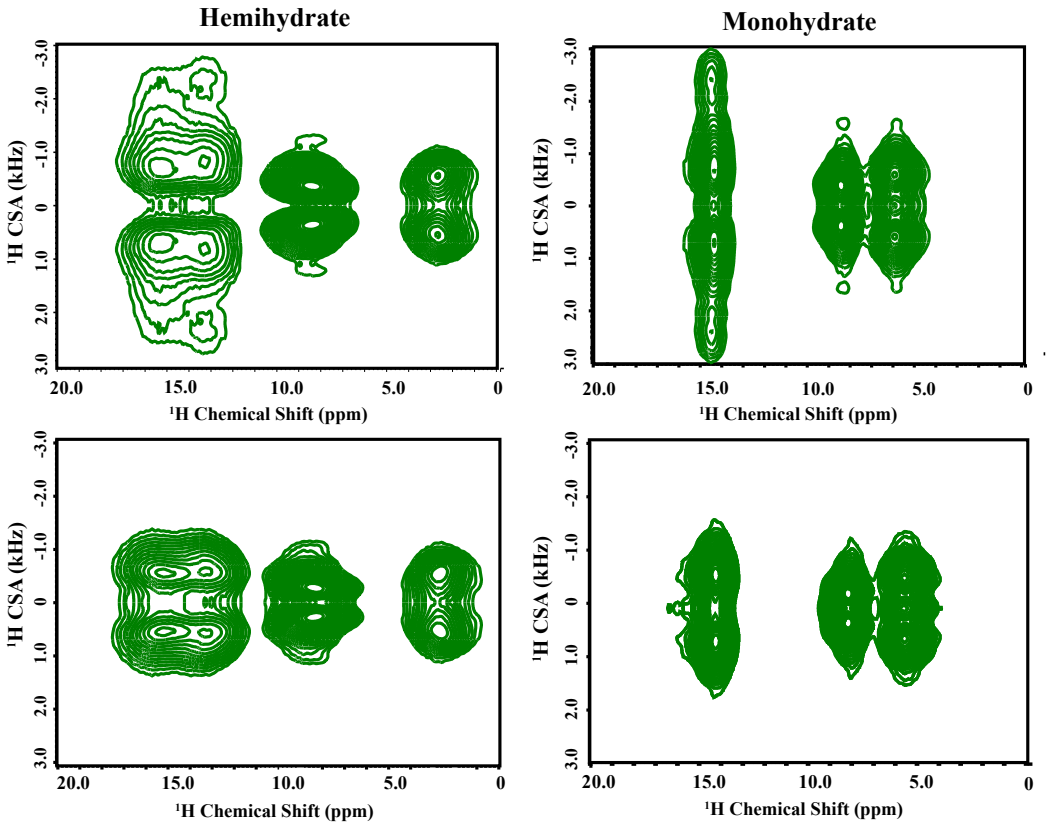

Figure S3. ^{1}H CS/CSA correlation recorded with (bottom) and without (top) ^{14}N decoupling. The downfield resonances are clearly most influenced by the presence of ^{14}N heteronuclear dipolar interaction identifying those as directly bonded.

Table S3. Comparison of ^{1}H CSA values with and without ^{14}N decoupling.

Hemihydrate	**NH**	**NH**	**Ar (overlap)**	**H_2O (overlap)**
δ_{iso} (ppm)	15.17	13.23	8.34	2.75
ζ (ppm)	10.2	11.6	5.2	9.6
η	0.75	0.8	0.85	0.6
ζ (ppm) w/o dec	--	--	6.7	9.9
η w/o dec			0.7	0.65
Monohydrate	**NH (overlap)**	**Ar (overlap)**	**H_2O (overlap)**	
δ_{iso} (ppm)	14.4	8.45	5.9	
ζ (ppm)	11.3	5.5	10.2	
η	0.7	0.85	0.75	
ζ (ppm) w/o dec	--	7.1	10.6	
η w/o dec	--	0.7	0.75	

SI 4. Infrared Spectroscopy

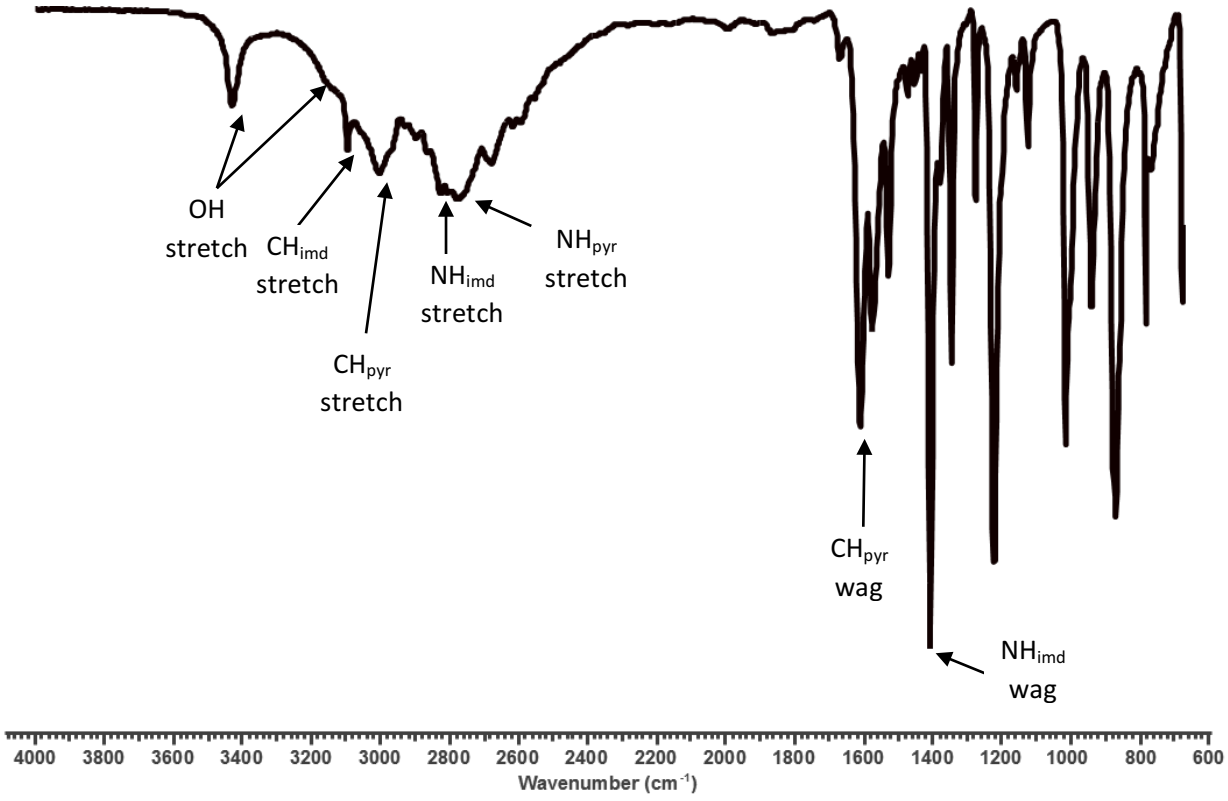

Figure S4. Experimental IR spectrum of the monohydrate form of mercaptopurine with labels based on computational predictions. [Note: imd=imidazole ring, pyr=pyrimidine ring]

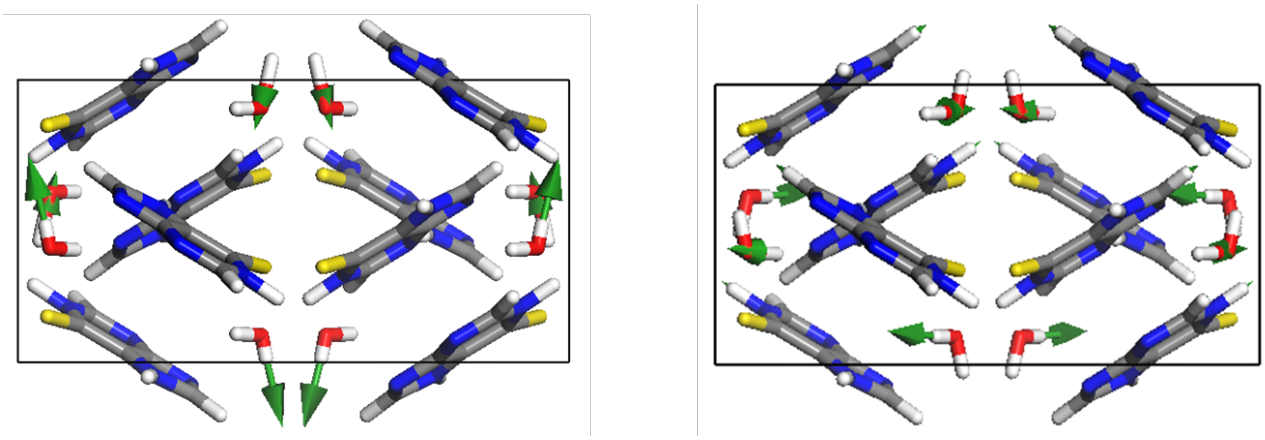

Figure S5. Structural depiction of the calculated stretching for the OH hydrogen bound to sulfur (left, 3428.9 cm^{-1} experimentally) and the OH hydrogen bound to nitrogen (right, ~3160 cm^{-1} experimentally) for the monohydrate form of mercaptopurine.

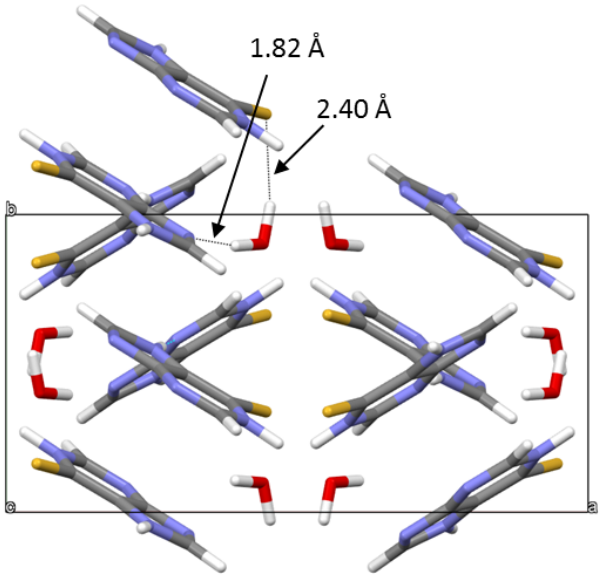

Figure S6. Structural depiction of the experimental unit cell of the monohydrate form of mercaptopurine with the OH hydrogen bonds highlighted (OH···S is 2.40 Å, OH···N is 1.82 Å).

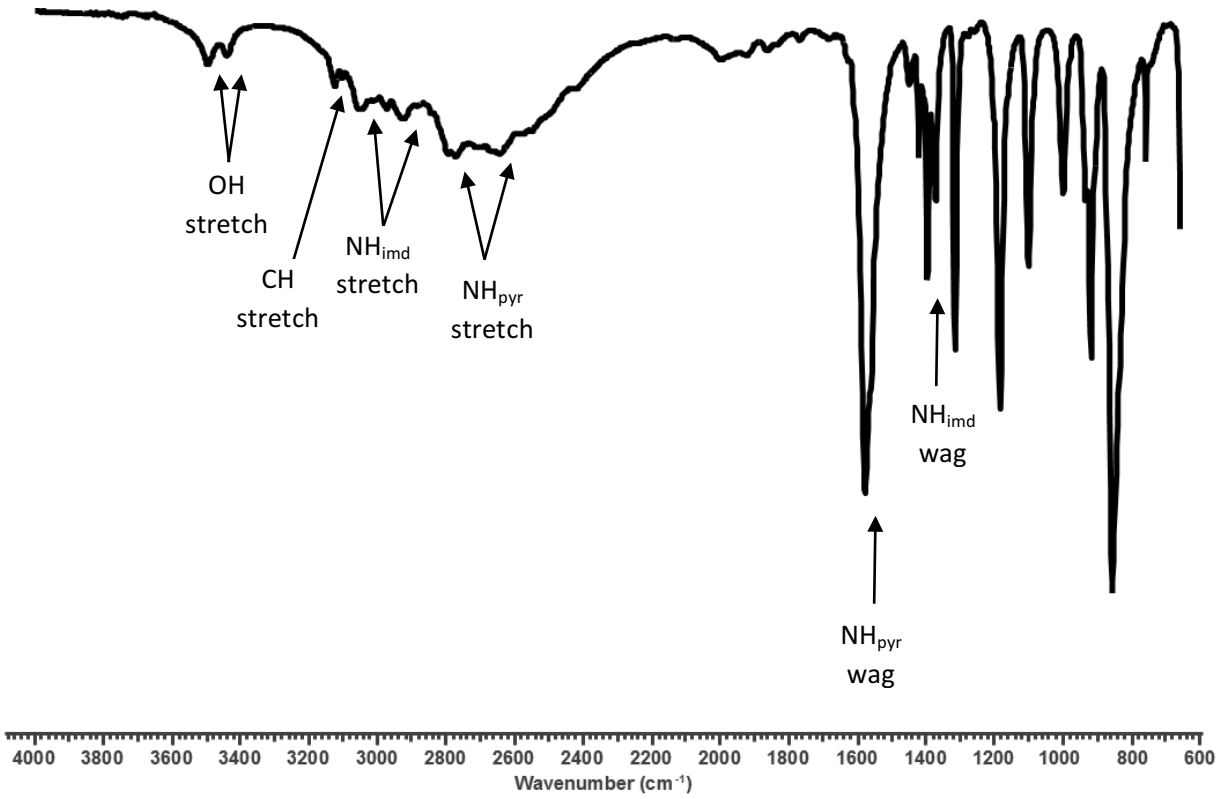

Figure S7. Experimental IR spectrum of the hemihydrate form of mercaptopurine with labels based on computational predictions. [Note: imd=imidazole ring, pyr=pyrimidine ring]

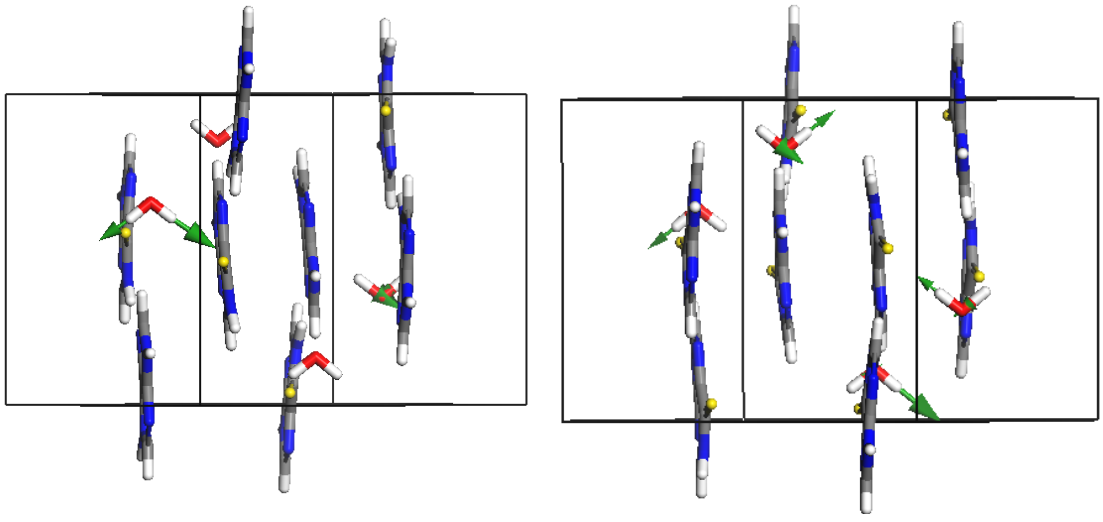

Figure S8. Structural depiction of the symmetric OH stretching (left, 3444.4 cm^{-1} experimentally) and asymmetric OH stretching (right, 3500.3 cm^{-1} experimentally) calculated for the hemihydrate form of mercaptopurine.

SI 5. Theoretical calculation data for mercaptopurine hydrate forms

Theoretical Desolvation Energy Calculations

The crystal structure for the monohydrate form was taken from the Cambridge Structural Database (RefCode: MERPUM)[12]. The crystal structure for the hemihydrate form was solved in house. All modules used were part of the Materials Studio 7.0 suite. Bonds were calculated if necessary and correct bond orders were assigned based on the crystal structures. The following procedures were optimized based on previous literature.[13]

Figure S9. Depiction of how the theoretical desolvation energy calculations were derived.

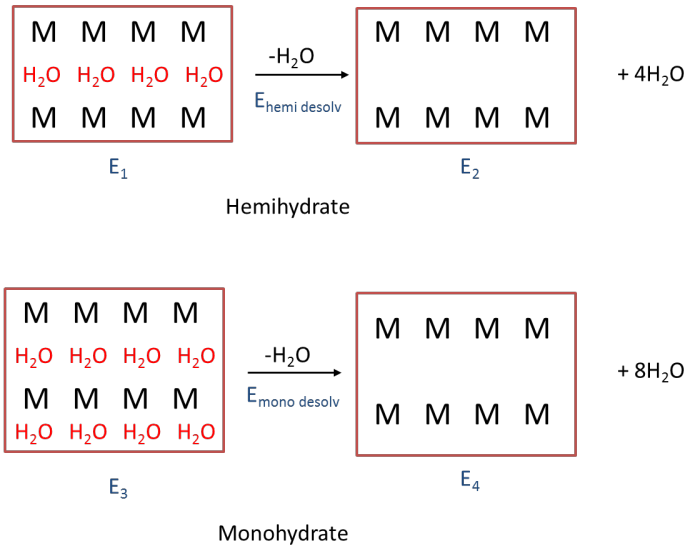

Using the concept that the energy of the desolvation process is products – reactants, this gives the following two equations:

$4\,H_2O + E2 - E1 = E_{hemi\ desolv}$ (1)

$8\,H_2O + E4 - E3 = E_{mono\ desolv}$ (2)

Rearranging equation 1 for the water gives:

$4\,H_2O = E_{hemi\ desolv} - E2 + E1$ (3)

Multiplying equation 3 by 2 and substituting in for $4H_2O$ in equation 1 gives:

$E4 + \{2[E_{hemi\ desolv} - E2 + E1]\} - E3 = E_{mono\ desolv}$ (4)

Rearranging equation 4 gives equation 5, in which we can calculate the difference in desolvation energies between the two forms (in terms of the number of water molecules per structure) based on the 4 energies which were calculated using the above computational methods:

$$E4 - E3 - 2E2 + 2E1 = E_{mono\ desolv} - 2E_{hemi\ desolv} \quad (5)$$

Table S4 shows the energies for each structure (E1-E4) calculated by each of the three computational methods. The results of equation 5 for each method are shown in Table S5. The magnitude of each calculation is different, which shows that each computational method takes different interactions into account. However, each method shows that the monohydrate has a higher theoretical desolvation energy, indicating that the water molecules are held in more tightly from an energetic standpoint (i.e. more strongly hydrogen bound) than the water molecules in the hemihydrate.

Table S4. Geometry optimization and energy calculations for the two hydrate forms of mercaptopurine using three different computational methods.

Method	Forcite (E1)	Forcite (E2)	CASTEP (E1)	CASTEP (E2)	Dmol3 (E1)	Dmol3 (E2)
Energy	402.47	164.54	-449,930.31	-406,551.36	-4,259,328.10	-4,067,404.30
	Forcite (E3)	Forcite (E4)	CASTEP (E3)	CASTEP (E4)	Dmol3 (E3)	Dmol3 (E4)
Energy	637.31	272.42	-493,311.58	-406,483.05	-4,451,283.30	-4,067,335.30

Table S5. Difference in theoretical desolvation energies calculated from the values in table S4 using equation 5 above. These values represent $E_{mono\ desolv} - 2E_{hemi\ desolv}$.

Computational method	Forcite	CASTEP	Dmol3
Energy per unit cell (kcal/mol)	110.97	70.63	100.40
Energy per water molecule (kcal/mol)	13.87	8.83	12.55

SI 6. References

[1] K. M. Kersten, A. J. Matzger, *Chem. Commun.* **2016**, *52*, 5281–5284.

[2] M. K. Pandey, Y. Nishiyama, *J. Magn. Reson.* **2015**, *261*, 133–140.

[3] M. K. Pandey, M. Malon, A. Ramamoorthy, Y. Nishiyama, *J. Magn. Reson.* **2015**, *250*, 45–54.

[4] M. H. Levitt, *Encycl. Nucl. Magn. Reson.* **2002**, *9*, 165–196.

[5] M. Carravetta, M. Edén, X. Zhao, A. Brinkmann, M. H. Levitt, *Chem. Phys. Lett.* **2000**, *321*, 205–215.

[6] T. Brown, "100 Best-Selling, Most Prescribed Branded Drugs Through March," can be found under http://www.medscape.com/viewarticle/849457, **2015**.

[7] "Top 100 Drugs for 2013 by Units Sold," can be found under https://www.drugs.com/stats/top100/2013/units, **2014**.

[8] "Top 100 Drugs for 2011 by Units Sold," can be found under https://www.drugs.com/stats/top100/2011/units, **2014**.

[9] "Top 200 Drugs by Units Sold (2005) - Drugs.com," can be found under https://www.drugs.com/top200_units_2005.html, **2014**.

[10] "Top 200 Drugs by Units Sold (2009) - Drugs.com," can be found under https://www.drugs.com/top200_units_2009.html, **2014**.

[11] "Top 200 Drugs by Units Sold (2007) - Drugs.com," can be found under https://www.drugs.com/top200_units_2007.html, **2014**.

[12] C. R. Groom, I. J. Bruno, M. P. Lightfoot, S. C. Ward, IUCr, *Acta Crystallogr. Sect. B Struct. Sci. Cryst. Eng. Mater.* **2016**, *72*, 171–179.

[13] K. R. Mitchell-Koch, A. J. Matzger, *J. Pharm. Sci.* **2008**, *97*, 2121–2129.